**Annales
Geophysicae**

Different responses of northern and southern high latitude ionospheric convection to IMF rotations: a case study based on SuperDARN observations

D. Ambrosino[1], **E. Amata**[1], **M. F. Marcucci**[1], **I. Coco**[1], **W. Bristow**[2], and **P. Dyson**[3]

[1]Istituto di Fisica dello Spazio Interplanetario, IFSI – INAF, Roma, Italy
[2]Geophysical Institute, UAF, USA
[3]La Trobe Un., Victoria, Australia

Abstract. We use SuperDARN data to study high-latitude ionospheric convection over a three hour period (starting at 22:00 UT on 2 January 2003), during which the Interplanetary Magnetic Field (IMF) flipped between two states, one with $B_y \gg |B_z|$ and one with $B_z > 0$, both with negative B_x. We find, as expected from previous works, that day side ionospheric convection is controlled by the IMF in both hemispheres. For strongly northward IMF, we observed signatures of two reverse cells, both in the Northern Hemisphere (NH) and in the Southern Hemisphere (SH), due to lobe reconnection. On one occasion, we also observed in the NH two viscous cells at the sides of the reverse cell pair. For duskward IMF, we observed in the NH a large dusk clockwise cell, accompanied by a smaller dawn cell, and the signature of a corresponding pattern in the SH. On two occasions, a three cell pattern, composed of a large clockwise cell and two viscous cells, was observed in the NH. As regards the timings of the NH and SH convection reconfigurations, we find that the convection reconfiguration from a positive B_z dominated to a positive B_y dominated pattern occurred almost simultaneously (i.e. within a few minutes) in the two hemispheres. On the contrary, the reconfiguration from a B_y dominated to a northward IMF pattern started in the NH 8–13 min earlier than in the SH. We suggest that part of such a delay can be due to the following mechanism: as IMF $B_x < 0$, the northward-tailward magnetosheath magnetic field reconnects with the magnetospheric field first tailward of the northern cusp and later on tailward of the southern cusp, due to the IMF draping around the magnetopause.

1 Introduction

Ionospheric convection patterns resulting from reconnection at the Earth's magnetopause have been the object of a vast literature which has studied their dependence on Interplanetary Magnetic Field (IMF) orientation by means of low-altitude spacecraft (Heppner and Maynard, 1987; Weimer, 1995), ground magnetometers (Kamide et al., 1994; Papitashvili et al., 1994) and, more recently, SuperDARN convection measurements (Ruohoniemi and Greenwald, 1996, 2005; Chisham et al., 2007). On the other hand, a detailed understanding of high latitude ionospheric convection has been achieved in the course of years starting, for instance, from the seminal work of Cowley and Lockwood (1992).

For a southward IMF, reconnection takes place at the low latitude day side magnetopause, so that newly opened flux is transferred to the night side and two convection cells are set up in both hemispheres with anti-sunward flow in the polar caps. The relative dimensions and orientations of the two cells are known to depend upon the relative importance of the IMF B_z and B_y components: for $B_y > |B_z|$ dusk and dawn cells dominate in the Northern Hemisphere (NH) and in the Southern Hemisphere (SH) respectively; the opposite situation occurs when $B_y < B_z < 0$. In the extreme condition of a purely $B_y > 0$ field, Reiff and Burch (1985) forecast the formation of a single large clockwise cell in the NH and a counter-clockwise cell in the SH. Moreover, for all IMF conditions they forecast the presence of two lower latitude

Correspondence to: D. Ambrosino
(danila.ambrosino@ifsi-roma.inaf.it)

viscous cells, at dusk and dawn with respect to the main convection pattern over the central polar cap.

For strongly northward IMF, reconnection is thought to occur tailward of the cusps (lobe reconnection), thus generating two reverse cells with sunward flow over the polar cap. There has been disagreement in the past over the detailed patterns of ionospheric convection resulting from strongly northward IMF. Burke et al. (1979) and Reiff and Burch (1985) suggested the existence of four convection cells: two reverse cells at high latitudes driven by lobe reconnection, and two normal cells at lower latitudes driven by viscous processes at the magnetopause. On the contrary, Heppner and Maynard (1987) suggested that only two highly-distorted cells would develop, while Rich and Hairstone (1994) performed a statistical study and found that four-cell convection occurred very rarely. Conversely, Ruohoniemi and Greenwald (1996) using SuperDARN data showed that, on a statistical basis, a four-cell structure existed for strong northward IMF. Their statistical convection patterns clearly showed two reverse convection cells poleward of 80° MLAT near the noon meridian, which were almost completely contained within the day side ionosphere. In this regard, Milan et al. (2000) first used SuperDARN observations to infer the presence of a clockwise lobe cell for northward IMF with $B_y \simeq 0$, while Huang et al. (2000a) showed that the four cell convection configuration develops and is stable during steady northward IMF conditions.

Finally, the magnetic dipole tilt could favour lobe reconnection in the NH during the local summer and in the SH during the local summer. However, a large B_x is believed to alter this seasonal effect (Cowley, 1983; Crooker and Rich, 1993; Lockwood and Moen, 1999).

In the last few years, interest has been growing in comparing how northern and southern ionospheric convection respond to reconnection at the magnetopause. Amata et al. (2008) recently published a preliminary study of the day side ionospheric convection as a function of IMF orientation over a three hour interval when the IMF flipped between two states, positive B_y dominated and positive B_z, both with $B_x < 0$. In this paper, we study in more detail such a period, confirm quantitatively the suggestions made by Amata et al. (2008) and discuss them more thoroughly. Section 2 presents an overview of interplanetary and magnetosheath conditions during the period under study based on IMF and plasma data from the Advanced Composition Explorer (ACE) and magnetosheath magnetic field from Cluster 2; Sect. 3 briefly recalls the significance of SuperDARN data to the study of high latitude ionospheric convection; the response of day side convection to four IMF rotations is described in Sects. 4 and 5, in the NH and in the SH, respectively; Sect. 6 concentrates on measurements of the line of sight velocity by the Kodiak radar in the NH and by the TIGER radar in the SH between 11:00 and 12:00 MLT, showing that, when the IMF turns from dominant B_y to positive B_z, the NH and SH display different time responses; Sect. 7 presents a discussion

of the observations, while Sect. 8 gives a short summary of our findings.

2 Event overview

Figure 1 displays, from top to bottom, solar wind dynamic pressure, P_{dyn}, IMF B_x, B_y, B_z, in GSM, and clock angle (all as dashed lines) measured close to the L1 libration point, at (242.1; −18.6; 15.5) R_E GSM, by ACE for 160 min starting at 21:50 UT on 2 January 2003. The four lower panels also display B_x, B_y, B_z, in GSM, and the clock angle (as solid lines) as observed by Cluster spacecraft 2 (Balogh et al., 1997) in the magnetosheath during an outbound orbit between (−1.1; 0.9; 7.7) and (0.9; 4.4; 9.5) R_E GSM very close to the magnetopause, tailward and slightly duskward of the nominal location of the northern cusp. We shifted ACE data by 67 min to match the Cluster 2 B_z component after 23:25 UT; however, we notice that this shift does not yield a perfect alignment of the B_y components and of the clock angles. In fact, starting from 00:08 UT on 3 January 2003 the ACE B_y changed from positive to negative and then oscillated around 0 nT, while the Cluster 2 B_y dropped to 0 nT at 00:15 UT and then remained negative approching 0 nT from time to time. This discrepancy probably means that the IMF structures underwent some evolution between L1 and the Earth's orbit. Throughout the event, at ACE $B_x < 0$, while B_y was clearly positive, apart from short intervals when it approached 0 nT.

We notice that four major IMF rotations occurred, as evidenced by vertical solid lines. Line A, drawn at 22:07 UT, marks a rotation where the ACE clock angle, defined as $\theta = \arctan(B_y/B_z)$, changed from $\theta \simeq 45°$ to $\theta \simeq 90°$. At line B (22:45 UT) the ACE clock angle fell from $\theta \simeq 90°$ to $\theta \simeq 0°$ and then varied between $\theta \simeq 0°$ and $\theta \simeq 45°$ until the next clear rotation. At line C (23:18 UT) θ jumped to $\simeq 90°$. Line D is drawn at 23:49 UT, when Cluster 2 B_x turned negative, just when B_z rose from slightly negative values to zero; after that, a slow rotation occurred over about 15 min during which θ dropped from $\simeq 90°$ to $\simeq 0°$. The timing of the D rotation is reliable, because it is based on Cluster 2 IMF data in the magnetosheath close to the magnetopause and to the northern cusp. Conversely, the times when the other three IMF rotations reached the magnetopause cannot be exactly determined as, at those times, Cluster 2 was in the magnetosphere. Finally we remark that during the whole period the solar wind dynamic pressure generally increased from $\simeq 5.52$ to $\simeq 11.1$ nPa, which was due mainly to the increase of the solar wind number density, while the x component of the solar wind velocity was rather constant, $V_x \simeq -390$ km/s. The main increase of dynamic pressure occurred close to rotation A, from 5.1 to 8.12 nPa and a smaller increase occurred at rotation C, from 8.12 to 9.05 nPa; on the other hand, at rotation B the pressure decreased by 1.16 nPa to start increasing
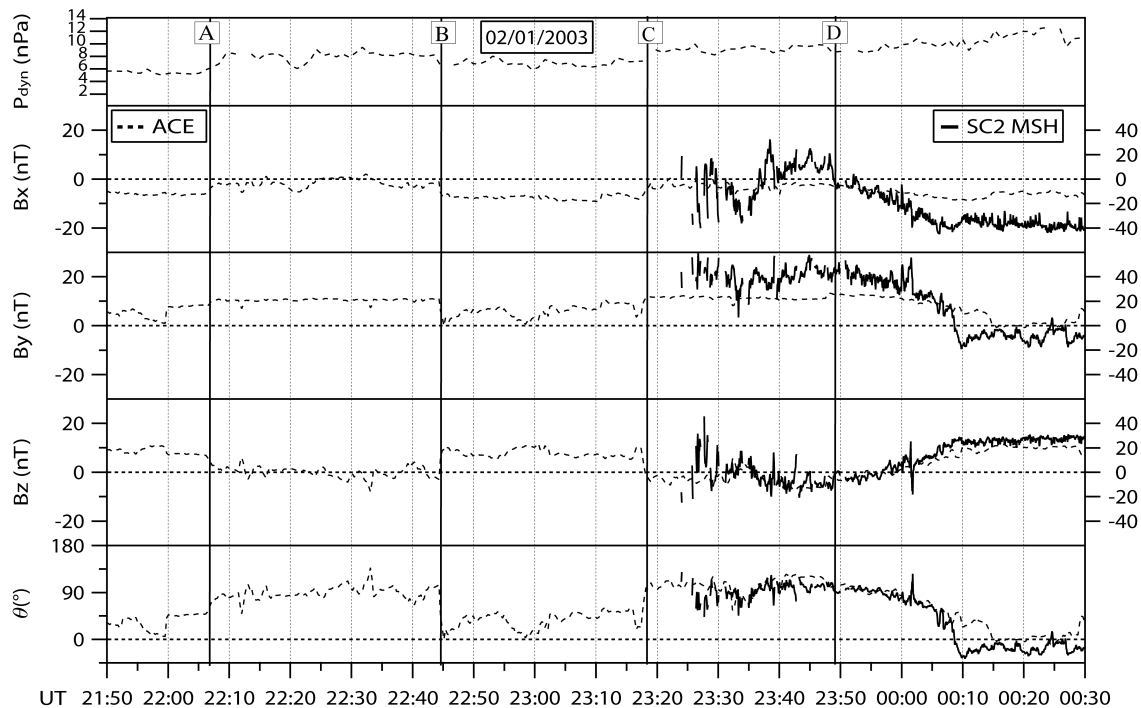
Fig. 1. From top to bottom: ACE dynamic pressure (computed by supposing that alpha particles contribute with a density equal to 4% of the proton density), GSM B_x, B_y and B_z and clock angle, defined as $\theta = \arctan(B_y/B_z)$, from ACE (dashed lines) and Cluster 2 in the magnetosheath (solid lines). The vertical solid lines mark the A, B and C IMF rotations and the start of the D rotation (see text for details). ACE data have been time shifted by 67 min. Dotted zero lines are also shown in the four lower panels.

again after a few minutes, while during the long D rotation it increased slightly from 8.82 to 9.74 nPa.

3 SuperDARN data and convection maps

The Super Dual Auroral Radar Network (SuperDARN) is a successful network of NH and SH HF radars to study the ionospheric convection in the auroral and polar regions (Greenwald et al., 1995; Chisham et al., 2007). Each radar, in the common mode of operation, performs measurements of the line of sight velocity (V_{LOS}) of the ionospheric plasma, between 90 and 400 km altitude, with a time resolution of 1 or 2 min, along 16 azimuthal beams separated by $\simeq 3°$, each consisting of 75 range gates between 180 and 3500 km from the radar site. The examination of the time evolution of V_{LOS} measured by each radar as a function of Magnetic Local Time (MLT) and magnetic latitude (MLAT) allows to pinpoint the response of high latitude convection to changes induced by interplanetary disturbances, e.g. IMF rotations. In addition, over many years a technique, called map potential, has been developed and extensively used to reconstruct NH and SH convection maps from SuperDARN data according to the method described by Ruohoniemi and Baker (1998) and Shepherd and Ruohoniemi (2000).

The performance of the map potential software critically depends on the SuperDARN data coverage. SuperDARN radars do not cover all MLT's and MLAT's, so that, even when valid echoes are available from a large portion of the radar fields of view (FOV), the map potential software makes use of additional data points determined by a statistical model of convection (Ruohoniemi and Baker, 1998; Ruohoniemi and Greenwald, 1996, 2005) to properly close the expansion in spherical harmonics. When the radar data coverage is good, the reconstructed maps over the regions where radar data are present are unequivocally determined by the actual measurements. On the other hand, as the data coverage reduces, the role played by the model increases and great care must be put in the interpretation of the reconstructed patterns.

During the period under study, data from 9 NH SuperDARN radars were available so that the NH coverage was good between $\simeq 65°$ and $\simeq 90°$ MLAT and from 09:00 MLT through 24:00 or even 03:00 MLT. In particular, on the day side data were provided by the King Salmon, Kodiak, Prince George, Saskatoon and Kapuskasing radars, while the Goose Bay, Stokkseyri, Thykkvibaer and Hankasalmi radars contributed to the convection maps on the evening side and on the night side. Starting from the available data we reconstructed NH convection maps throughout the event. In order
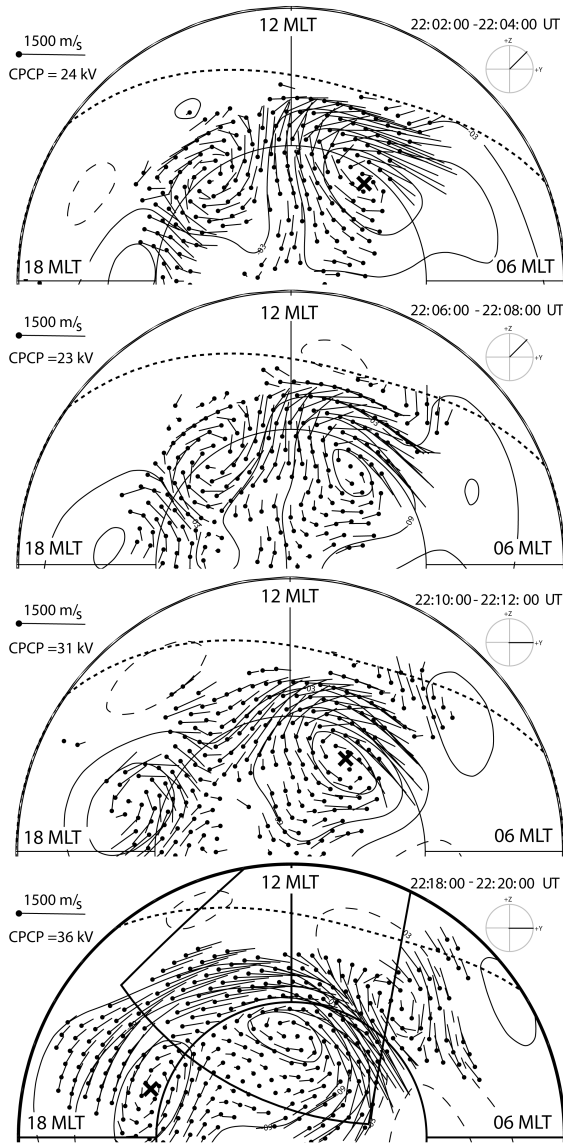
Fig. 2. SuperDARN NH dayside convection maps for rotation A of the IMF. The outer (inner) circle indicates 70° (80°) MLAT. The solid (dashed) curves indicate negative (positive) potential isocontours. The dotted line indicates the Heppner-Maynard boundary. The top left corner of each map shows the cross polar cap potential (CPCP) and a 1500 m/s vector according to which all vector lengths are scaled. The right hand top corner of each map shows the start and end times and a small inset indicating the IMF direction (according to Table 1) in the B_y-B_z GSM plane. The field of view of the Kodiak radar is overlaid to the bottom panel.

to do that, instead of using the individual time shifted IMF components shown in Fig. 1, we defined a number of time periods characterised by similar IMF conditions and calculated for each of them average values of the IMF components to be used as inputs to the map potential software. The result-

Table 1. IMF data used as inputs to the SuperDARN map potential software.

Time(UT)	B_x(nT)	B_y(nT)	B_z(nT)
22:00–22:07	−5	7.5	7.5
22:08–22:44	−3	10	0
22:45–23:18	−10	6.2	7.6
23:19–23:49	−3	10	−3
23:50–00:10	(−3; −7)	(10; 0)	(−3; 9)
00:10–00:50	−7	0	10

ing IMF data are shown in Table 1, which consists of 5 periods of constant IMF and 1 period (23:50–00:10 UT) during which each IMF component varied linearly with time. We recall that the map potential software chooses the convection statistical model on the basis of B_y, B_z and B (i.e. B_x is used for the calculation of B only). As a final test on the validity of the NH maps, we reconstructed them under two different conditions: a) using the IMF values listed in Table 1; b) using the Table 1 B_x and B_y values, but forcing $B_z = -3$ nT. As expected, apart from minor details, the maps did not change significantly, thanks to the large number of experimental data available throughout the period. In the next section, for each of the IMF rotations identified in Fig. 1 we will describe in detail the day side part of several maps calculated by using the IMF values of Table 1.

For the SH the coverage is much less: 5–9 MLT hours on the day side, mainly at dawn near noon MLT, between $\simeq -75°$ and $\simeq -85°$ MLAT, provided by the TIGER radar; 5–9 MLT hours on the night side, around midnight MLT, between $\simeq -75°$ and $\simeq -85°$ MLAT, provided by the Halley, Sanae, Syowa East and Syowa South radars. This means that, although enough data are available to reconstruct the general features of convection patterns thanks to the presence of data both on the day side and on the night side, on the day side such reconstructions must be regarded as qualitative. Therefore, in Sect. 5 we study the response of SH ionospheric convection to the IMF rotations mainly by looking at FOV plots of measured V_{LOS} to avoid any artefact from the statistical model used by the map potential software.

4 Effects of the IMF rotations on NH convection

4.1 The first rotation to dominant B_y

Figure 2 displays four NH day side convection maps for the 22:02–22:04, 22:06–22:08, 22:10–22:12, and 22:18–22:20 UT intervals. As we noted in the description of Fig. 1, apart from a 4 min period after 21:55 UT, the IMF already had a substantial B_y component prior to the 22:07 UT rotation. The main feature of the corresponding NH pattern (top panel) is a pair of reverse cells, centred at 15:00 MLT and 80° MLAT and at 09:30 MLT and 81° MLAT. Between

them a clear sunward flow heads from the polar cap along noon MLT and bends mainly towards dawn at 80° MLAT. The map also displays the signature of a small clockwise cell in the evening side, while no data are available in the 06:00–09:00 MLT region below 73° MLAT.

In the next 4 min the NH map does not change significantly, as illustrated by the 22:06–22:08 UT panel, apart from the appearance of a sunward flow at 09 MLT below 76° MLAT (resembling a portion of a counter-clockwise cell) and the strengthening of a clockwise partial dusk cell centred at 17:30 MLT and 76° MLAT (which are both fully reconstructed in the following convection maps). We interpret this pattern as composed of 2 reverse cells and 2 viscous cells (see e.g. Reiff and Burch, 1985).

The NH convection patterns show the start of a reconfiguration during the next 2 min (not shown), just at the time of the nominal IMF rotation (cf. Table 1). The reconfiguration then proceeded further as illustrated by the 22:10–22:12 UT map: the dusk side reverse cell has disappeared, but a clear sunward flow is still present from the polar cap around noon MLT. Moreover, we also notice the persistence of a sunward flow at 09:00 MLT below 76° MLAT (resembling a portion of a counter-clockwise cell) and the strengthening of the dusk clockwise cell at 17:00 MLT and 77° MLAT, which appears to be the evolution of the dusk evening cell partially reconstructed in the 22:02 and 22:06 UT maps.

In the next two min (not shown) the reconfiguration is complete, as the sunward flow from the polar cap disappears and a large clockwise cell centred at 82° MLAT and at noon MLT is established. This new convection pattern remains stable for about 20 min, as illustrated in the bottom panel at 22:18–22:20 UT. We see that the map now displays a clear three cell pattern, as the central noon MLT cell is accompanied by a dusk clockwise cell (focus at 17:00 MLT and 79° MLAT), which can be regarded as a "left over" of the dusk evening cell observed in the previous maps, and by a clear counter-clockwise cell at dawn (focus at 09:30 MLT and 77° MLAT).

In summary, in the NH the reconfiguration from $B_z > 0$ to dominant $B_y > 0$ starts at 22:08 UT and ends at 22:14 UT.

4.2 The first IMF northward turning

Figure 3 displays five NH day side convection maps for the 22:36–22:38, 22:46–22:48, 22:54–22:56, 23:00–23:02 and 23:04–23:06 UT intervals. The top panel shows that, prior to the IMF rotation, the NH convection pattern exhibited a large dusk clockwise cell centred at 13:00 MLT and 83° MLAT and a smaller counter-clockwise dawn cell separated by a clear anti-sunward and dawnward flow extending from 77° MLAT and 13:00 MLT to 82° MLAT and 09:00 MLT. Such a pattern clearly results from the evolution of that shown in the bottom panel of Fig. 2.

The next three 2-min maps, which we do not show, present evidence of a slow evolution of the NH convection pattern.
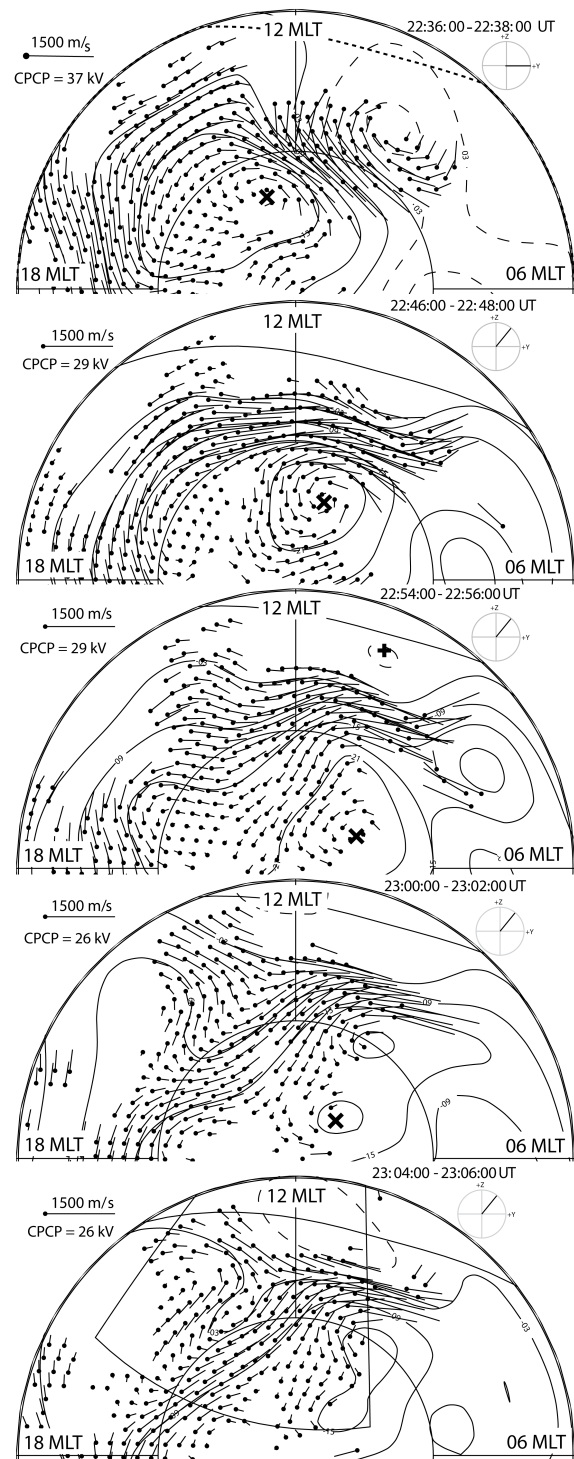
Fig. 3. SuperDARN NH dayside convection maps for rotation B of the IMF. Same format as in Fig. 2.

Eventually, the 22:46–22:48 UT map shows: a) a clockwise cell centred at noon MLT and 83° MLAT (producing a sunward flow at 82°−84° MLAT and 12:00–13:00 MLT), b) a
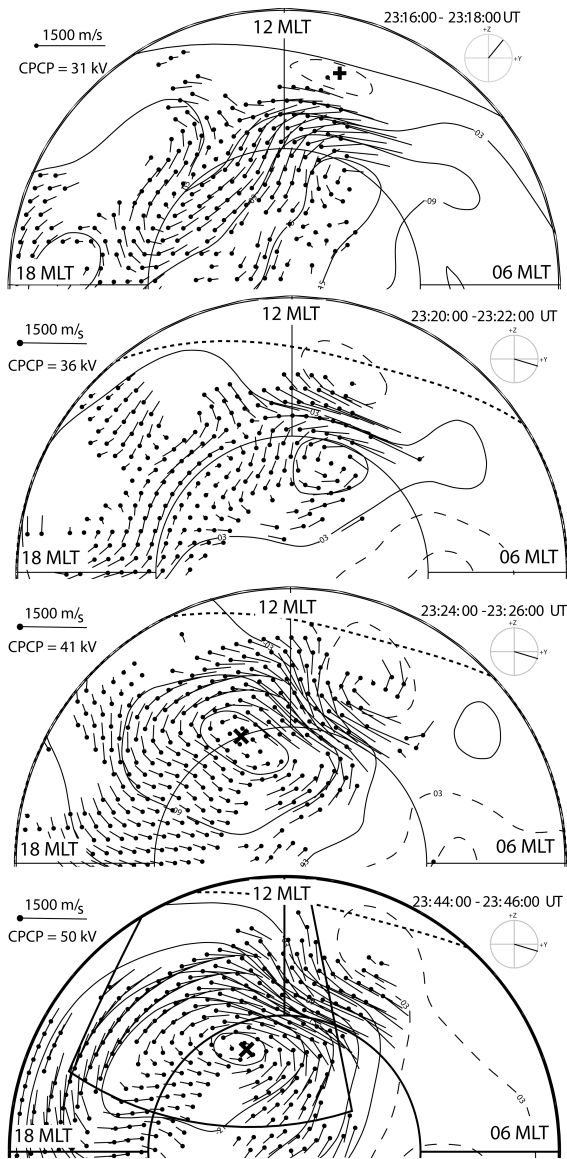
Fig. 4. SuperDARN NH dayside convection maps for rotation C of the IMF. Same format as in Fig. 2.

small clockwise cell at dusk with focus at 81° MLAT and 16:00 MLT, c) a portion of the dawn cell (which seems to have moved sunward), d) a mainly dawnward flow extending from 15:00 to 09:00 MLT at 77°−80° MLAT.

In the next 8 min the NH pattern further evolves and the noon MLT cell shifts toward dawn (Huang et al., 2000a). At 22:54–22:56 UT (third panel from the top) the focus of this cell is located at 85° MLAT and 08:30 MLT, while the clockwise cell centred at 81° MLAT and 16:00 MLT has faded. At the same time the dawn counter-clockwise cell is not visible any more.

In the next 4 min (not shown) the sunward flow around noon MLT between 80° and 90° MLAT widens in MLT and the signature of a counter-clockwise cell appears centred at 14 MLT and 78° MLAT, as illustrated in the fourth panel from the top (23:00–23:02 UT). Moreover, the dusk quadrant displays the signature of a clockwise vortex stretching from 13:00–18:00 MLT, probably due to a large viscous cell. The final result of this evolution is shown in the bottom panel (23:04–23:06 UT). The main features of this NH map are: a) a sunward flow extending from high latitude in the polar cap and crossing 82° MLAT from 09:00 to 13:00 MLT, b) the mainly dawnward flow across noon MLT at 77° MLAT, c) the new partial counter-clockwise cell centred at 13:30 MLT and 78° MLAT; d) the signature of a dusk viscous cell. Although we do not see two clear reverse cells, there is no doubt that this pattern is due to reconnection tailward of the NH cusp.

In summary, in the NH the reconfiguration from dominant $B_y > 0$ to $B_z > 0$ starts around 22:45 UT and ends at 23:02 UT.

4.3 The second rotation to dominant B_y

Figure 4 displays four NH dayside convection maps for the 23:16–23:18, 23:20–23:22, 23:24–23:26, and 23:44–23:46 UT intervals. The top panel map shows the last convection map before the nominal 23:18 UT IMF rotation and is similar to the three preceding ones (which we do not show). As it can be seen from Fig. 1, between 22:26 and 23:18 UT the IMF already slowly rotated and a substantial B_y component had developed. The main feature of the top panel NH pattern is the sunward flow which heads from the polar cap (slightly from the dusk side) along noon MLT and bends towards dawn at 80° MLAT, thus suggesting the existence of a clockwise lobe cell, not fully resolved due to the lack of data in the first half of the dawn quadrant. The signature of a partial clockwise cell is seen in the dusk quadrant centred at $\simeq 77°$ MLAT and 14:30 MLT. Moreover, a clockwise cell is seen centred at 17:30 MLT and $\simeq 73°$ MLAT. Such a pattern clearly results from the evolution of the ones shown in the bottom panel of Fig. 3.

In the next 2 min we see evidence that the convection pattern is changing. This is the time of the nominal IMF rotation (cf. Table 1) and a transient clockwise cell appears centred at 82° MLAT and 11:00 MLT which is limited at lower latitudes by the pre-existing dawnward flow around noon MLT and at higher latitudes by a duskward and slightly tailward flow. As part of the pattern evolution, the partial counter-clockwise cell centred at $\simeq 79°$ MLAT and 14:00 MLT has disappeared, while the clockwise cell formerly centred at 17:30 MLT and $\simeq 73°$ MLAT has faded and moved slightly sunward.

The reconfiguration is complete in the next map (not shown) and can be seen in the third panel from the top (23:24–23:26 UT): the sunward flow around noon MLT has disappeared and a large clockwise dusk cell extends partially to the dawn quadrant; moreover, a smaller dawn cell appears

separated from the dusk cell by a dusk-dawn and tailward flow across noon MLT at 75°−80° MLAT. This situation remains essentially unchanged in the next 25 min, as illustrated by the bottom panel (23:44–23:46 UT).

In summary, this reconfiguration from $B_z > 0$ to dominant $B_y > 0$ starts at 23:18 UT and ends at 23:24 UT.

4.4 The second IMF northward rotation

Figure 5 displays five NH day side convection maps for the 23:58–00:00, 00:06–00:08, 00:16–00:18 UT, 00:18–00:20 and 00:26–00:28 UT intervals. A slow rotation of the IMF starts at 23:49 UT (see Fig. 1) and makes the Cluster 2 clock angle drop from 90° to below 0° in 20 min. The effects of this rotation in the convection maps show up gradually. In fact, the NH convection pattern for 23:58–00:00 UT (top panel) shows a large dusk clockwise cell extending to the dawn quadrant, which is still clearly due to B_y dominated reconnection and looks like the evolution of the pattern in the bottom panel of Fig. 4.

In the next six minutes, similarly to what was observed for the first northward IMF rotation, an evolution of the NH pattern is observed until a sunward flow develops at 80°−85° MLAT and 11:00–13:00 MLT, which appears to deflect towards the Sun the dawn-dusk flow at lower latitudes. This can be seen in the 00:06–00:08 UT panel, i.e. when the clock angle was $\simeq 45°$ (see Fig. 1) and the Cluster 2 $B_z \simeq 5$ nT.

The following four 2-min NH maps all display a dusk-dawn flow at 75°−78° MLAT and 11:00–13:00 MLT and a sunward flow from the polar cap down to $\simeq 80°$ MLAT around noon MLT, while the IMF has completed its northward rotation at 00:10 UT. At 00:16–00:18 UT, a counter-clockwise cell starts developing at dusk, centred at 76° MLAT and 14:30 MLT, while the dawn-dusk flow around noon MLT appears reduced in extension and intensity. At 00:18–00:20 UT the next map shows that the dusk side counter-clockwise cell centred at 14:30 MLT has fully developed.

In the following minutes the NH maps keep a constant topology, but for the emergence of a large clockwise cell, centred at 17:00 MLT and 73° MLAT, which can be probably attributed to a viscous cell, as illustrated by the 00:26–00:28 UT map displayed in the bottom panel. The main feature of such map is the dusk counter-clockwise cell roughly at the centre of the dusk quadrant, which can be interpreted as the dusk cell of the expected two reverse cell system, while the dawn cell cannot be resolved due to the lack of data coverage. We also notice that the dawnward flow at 10:00–12:00 MLT continues to fade, until, after 00:30 UT (not shown), it ceases completely.

In summary, the last NH reconfiguration from $B_y > 0$ dominated to $B_z > 0$ dominated starts at 00:04 UT and ends at 00:20 UT.
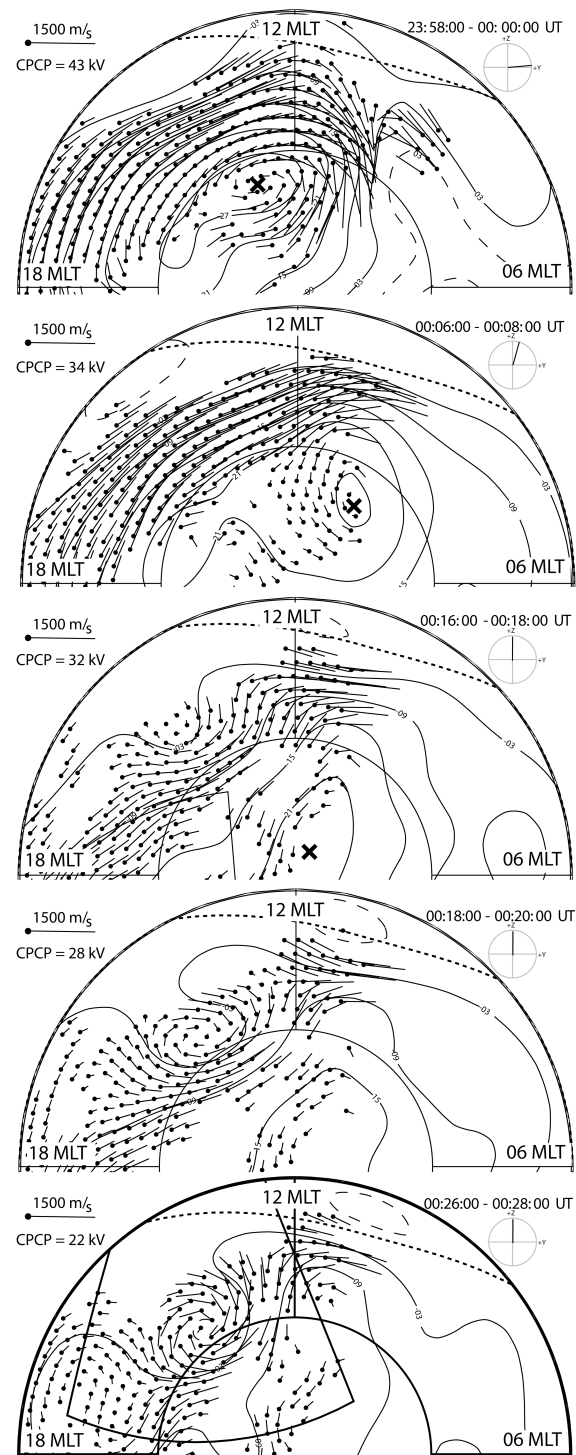
Fig. 5. SuperDARN NH day side convection maps for rotation D of the IMF. Same format as in Fig. 2.
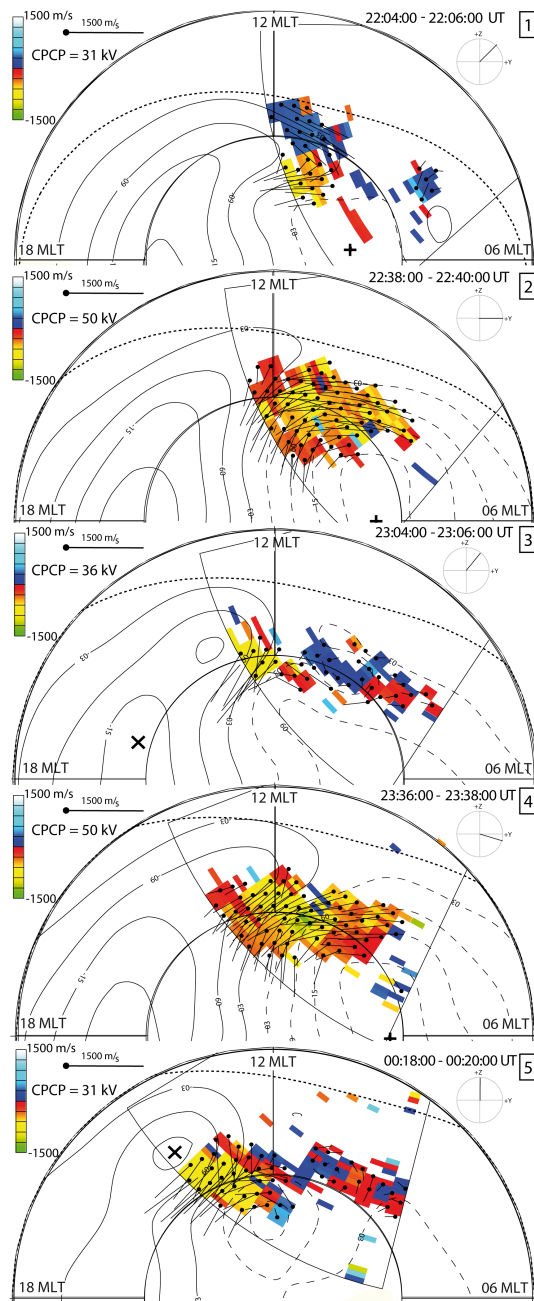
Fig. 6. Line of sight velocities measured by TIGER in the SH during five 2 min scans corresponding to different IMF conditions. The outer (inner) circle indicates −70° (−80°) MLAT. The TIGER field of view and convection maps with computed vector velocities are overlaid to each panel: the solid (dashed) curves indicate negative (positive) potential isocontours, while the dotted line indicates the Heppner-Maynard boundary. The top left corner of each map shows: a palette according to which velocities are colour coded, the cross polar cap potential (CPCP); a 1500 m/s vector according to which all vector lengths are scaled. The right hand top corner of each map shows the start and end times and a small inset indicating the IMF direction (according to Table 1) in the B_y-B_z GSM plane.

5 Effects of the IMF rotations on SH convection

As we remarked already in Sect. 3, only TIGER data are available in the SH day side. Therefore, we visually inspected all 2-min FOV plots of the TIGER V_{LOS} for the whole period under study. We will not show and describe all such plots, but we concentrate on five of them, which are contained as individual panels in Fig. 6 and display V_{LOS} as colour coded cells plotted in polar coordinates between −70° and −90° MLAT and from 06:00 to 18:00 MLT. In such a representation the Sun is at the top, the radar site is outside the figure in the morning quadrant, at −55.31° MLAT and 133.96° West geomagnetic longitude, the radar FOV is indicated by a fan bounded by black solid lines, and velocities towards (from) the radar are positive (negative). Each panel is typical of one of the five periods defined in Fig. 1. In addition to the measured velocities, each panel also shows the potential isocontours calculated through the map potential software together with velocity vectors calculated at points where actual measurements are available. Such maps are built by making use also of the SuperDARN data which are available in the night side. However, as the maps on the day side are only based on TIGER data, we do not assign to them a quantitative meaning.

The top panel refers to the 22:04–22:06 UT interval, just before the A rotation, and displays a clear region of cells characterised by positive velocity between ≃ −77° and ≃ −81° MLAT and between 10:30 and 12:00 MLT, which is adjacent to a region at higher MLAT where velocities are negative. Further to such regions, some scattered velocities are present at lower MLT, heading towards the radar at lower MLAT and away from it at higher MLAT. Similar velocity patterns are observed by TIGER in all two-min intervals before the A rotation.

At the A rotation the situation changes and a new velocity pattern is attained within a few minutes. An example of the new pattern is shown in the second panel from the top which refers to the 22:38–22:40 UT interval, when the IMF clock angle was ≃ 90° MLAT. In this case we see that practically all measured velocities are directed away from the radar. Moreover, the number of back-scattering cells has considerably increased, by roughly a factor 2.

At the B rotation the situation changes again, but the old velocity pattern persists for several minutes, and a new one emerges starting from 22:58 UT, until a clear region of positive velocity is set up between ≃ −77° and ≃ −80° MLAT between 09:00 and 11:30 MLT, which is surrounded by two regions of negative velocity at smaller and larger MLT, as shown in the third panel from the top (23:04–23:06 UT). At the same time the number of echoes observed in the TIGER FOV drastically drops. We also notice that the map potential software reconstructs, during several 2 min scans, a small clockwise cell in the dawn quadrant, centred at 11:00 MLT and −82° MLAT.

A new clear change of velocity pattern occurs immediately after the C rotation, as shown by the fourth panel from the top, which refers to the 23:36–23:38 UT interval, when the IMF clock angle and that measured in the magnetosheath by Cluster 2 were both $\simeq 90°$. Again, as for the 22:38–22:40 UT interval, the measured velocities are almost all directed away from the radar and are consistent with the new IMF orientation, while the number of echoes has roughly doubled again.

Finally, at the D rotation the last change of pattern takes place. Again the reconfiguration in the SH starts at 00:12 UT, 8 min later than in the NH, until a region of positive velocities sets up around 11:00 MLT, similarly to what was observed after the B rotation. The decrease of the number of echoes occurs again, although not so dramatically as for the B rotation. Again the map potential software reconstructs a small clockwise cell in the dawn quadrant.

In conclusion, we may state that: 1) as a consequence of each of the four IMF rotations, the TIGER V_{LOS} displays signatures which can be interpreted as due to convection reconfigurations; 2) more radar echoes are observed in the TIGER FOV for $B_z < 0$ or for dominant B_y than for $B_z > 0$; 3) after rotations A and C the reconfiguration starts within a few minutes, as in the NH, while after rotations B and D it starts several minutes later than in the NH.

6 Kodiak and TIGER V_{LOS} reversals

In the preceding two sections, based on SuperDARN convection maps for the NH and on TIGER FOV plots for the SH, we showed evidence that day side convection in both hemispheres reconfigured as a consequence of IMF rotations. Moreover, if we compare the reconfiguration times quoted for the NH in Sect. 4 and for the SH in Sect. 5, we notice that the reconfiguration seems to have occurred at different times in the two hemispheres at the two northward rotations of the IMF.

As we noticed already in the description of Figs. 2, 3, 4 and 5, the NH reconfiguration always seems to start close to 12:00 MLT and at latitudes close or above 80° MLAT. On the other hand, the change observed in Fig. 6 in relation to the IMF rotations regarded the sign of V_{LOS} close to $-80°$ MLAT and between 10:30 and 12:00 MLT. This suggests that, in order to summarise the information on reconfiguration times with a single figure, it is worthwhile examining directly V_{LOS} as measured by single radars in such MLAT-MLT regions.

We recall that the bottom panels of Figs. 2, 3, 4 and 5 and all panels of Fig. 6 show the FOV's of the Kodiak and TIGER radars superimposed on the NH and SH convection maps, respectively. NH data were also available from radars other than Kodiak and were used in the reconstruction of the potential maps; however, it appears that the Kodiak FOV was roughly pointing towards the north magnetic pole close to the noon MLT meridian. For the Kodiak data around noon MLT

positive velocities (towards the radar) correspond to sunward flows (from the polar cap to lower MLAT) and negative velocities (away from the radar) correspond to tailward flows (from low latitudes towards the polar cap). On this basis, we expect to see signatures of the flow reconfigurations in the time series of Kodiak V_{LOS} near noon MLT, i.e. normal convection cells should yield negative velocities and reverse cells should yield positive velocities.

As regards the SH, the TIGER FOV was on average at a 60° angle from noon MLT during the A rotation and at about 30° during the D rotation. As a consequence, one can expect that signatures of reconfigurations, in the form of V_{LOS} reversals, should show up as well in the time series of TIGER V_{LOS} near noon MLT and should be more and more evident as the angle between the TIGER beams and the 12:00 MLT meridian decreases.

Concerning the examination of V_{LOS} as a function of time, a further problem stems from the fact that each radar beam samples different MLT's as a function of time. In order to remove this ambiguity, we considered the 11:00–12:00 MLT sector and two 2° MLAT bins, from 78° to 80° MLAT in the NH and from $-78°$ to $-80°$ MLAT in the SH, we excluded ground scatter and all echoes having a reflected power <3 dB and averaged V_{LOS} for each 2 min interval. In this way we produced two time series of V_{LOS}, which we will hereafter call V_T for TIGER and V_K for Kodiak.

Figure 7, in its upper panel, displays V_T and V_K from 22:00 UT, 2 January 2003, to 00:30 UT, 3 January 2003, thus including the A, B, C and D IMF rotations (marked with vertical dashed lines). Moreover, the lower panel of Fig. 7 displays the number of valid echoes (i.e. excluding ground scatter and reflected power < 3 dB) over the whole TIGER and Kodiak FOV's, indicated by N_T (black solid line) and N_K (black dashed line), respectively. As during the whole event, the Kodiak and TIGER radars operated with 1 and 2 min resolution, respectively, the number of Kodiak echoes has been divided by 2.

It appears that both V_T and V_K in Fig. 7 alternate between positive and negative values. In particular, as regards V_T three "positive" periods are seen with average values ranging from 300 m/s to 150 m/s and with oscillations of the order of 50 m/s, while in the two "negative" periods the average values range from -300 to -700 m/s, with oscillations usually of the order of 100 m/s (apart from one large oscillation which reaches a peak-to-peak value of 500 m/s around 22:50 UT). A similar behaviour is displayed by V_K, with "positive" averages ranging from 500 to 100 m/s, while the "negative" averages are -400 and -500 m/s; in this case the oscillations are somewhat larger, i.e. 100–500 m/s peak-to peak. However, the maxima of both V_T and V_K during the "negative" periods fall well below (by a few hundred m/s) the minima of the "positive" periods. We interpret the positive values of V_T and V_K in terms of flow separating two reverse cells characteristic of lobe reconnection due to a northward IMF, and the negative values as anti-sunward flow towards
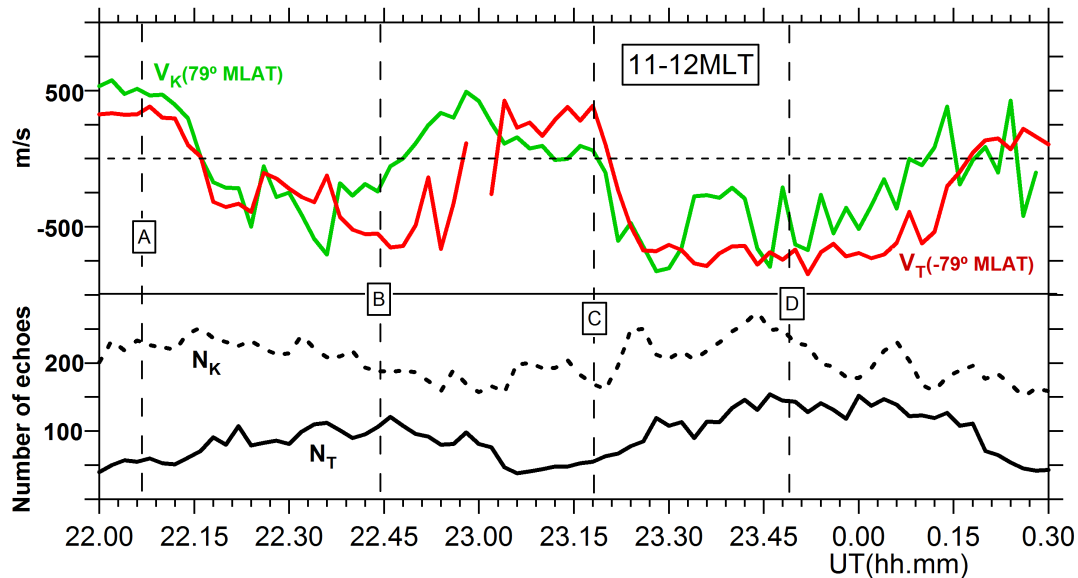
Fig. 7. Upper panel: 11-12 MLT line of sight velocities as a function of time in two 2° MLAT bins, centred at 79° MLAT and at −79° MLAT, for Kodiak (V_K in green) and TIGER (V_T in red) radars, respectively. Lower panel: number of radar echoes over the whole TIGER and Kodiak fields of view, indicated by N_T and N_K, respectively (N_K divided by 2 to account for the 1 min resolution of Kodiak, compared with the TIGER 2 min resolution). The vertical dashed lines mark the A, B and C IMF rotations and the start of the D rotation (see Fig. 1).

the polar cap between two normal convection cells for dominant B_y. In fact, in the upper panel we notice that both V_T and V_K reverse, from positive to negative values, roughly at the same time, around 22:15 UT, about 8 min after the A rotation, and around 23:21 UT, about 3 min after the C rotation. On the contrary, V_K reverses from negative to positive at 22:48 UT, 4 min after the B rotation, about 15 min prior to the reversal experienced by V_T. Later on V_K turns positive about 18 min after the nominal D rotation, about 12 min prior to V_T.

Turning to the lower panel, we already noticed, from the visual inspection of all TIGER FOV's and convection maps, that the number of echoes appears to depend on the IMF orientation. In fact, we see that, although N_T undergoes variations of the order of 10–40 echoes from time to time, $N_T \simeq 50$ during the periods of northward IMF and $N_T \simeq 100-150$ during the B_y dominated periods. It also appears that, after the A and C rotations, N_T increases 6–9 min after the nominal rotation time, while, after the B and D rotations, N_T decreases 15–20 min after the nominal rotation time; i.e. the time lags between the IMF rotations and the main N_T changes are essentially the same as those between IMF and V_T. A quantitative way to describe this is to consider the cross correlation between N_T and V_T. This calculation yields that the linear correlation coefficient between N_T and V_T has a maximum value of −0.86 for a time lag of 2 min. A behaviour similar to that of N_T can also be recognised in the N_K plot: in fact, a minimum ($N_K \simeq 150$) can be identified between rotations B and C and after rotation D,

and a maximum ($N_K \simeq 270$) occurs before rotation D. However, no clear change of N_K occurs at the A rotation and N_K displays larger short lived excursion from the average trend than N_T. Therefore, we must conclude that in this case the correlation is worse, as it is confirmed quantitatively by the fact that the best linear correlation coefficient between N_K and V_K is −0.37 for a −4 min lag.

7 Discussion

In Sects. 4 and 5 we made use of SuperDARN observations to describe the response of day side ionospheric convection to four IMF rotations (see Fig. 1), during which the IMF flipped between a mainly $B_z > 0$ orientation and a mainly $B_y > 0$ with $B_z \simeq 0$ orientation, while B_x was always negative. As it was remarked in Sect. 2, the IMF rotations were accompanied by variations of the solar wind dynamic pressure, which overall increased from 5.52 to 11.1 nPa from the start to the end of the period under study. Newell and Meng (1994) showed that, when $P_{dyn} < 2$ nPa, the NH cusp is located on average about noon MLT and 80° MLAT with widths of 01:00 MLT and 3° MLAT, while, when $P_{dyn} > 4$ nPa, it is located on average about noon MLT and 78° MLAT with widths of 03:00 MLT and 9° MLAT. This statistical behaviour suggests that an increased solar wind dynamic pressure favours the transfer of mass and energy through the magnetopause; this, in turn, should result in enhanced ionospheric convection. On these grounds, we do not expect that at rotations B and D the dynamic pressure played

a role in determining the different reconfiguration times observed in the two hemispheres. This consideration is justified by the fact that the pressure behaved differently at such two rotations: in fact, at rotation B it decreased slightly from 7.9 to 6.7 nPa to start increasing again after a few minutes, while during the long D rotation it only increased moderately from 8.8 to 9.7 nPa. A similar pressure increase, from 8.1 to 9.0 nPa, was observed at rotation C, but in this case no time lag occurred between the NH and SH reconfigurations. Finally, the largest effect on ionospheric convection during the whole period under study should be expected at rotation A, at which the pressure jumped from 5.1 to 8.1 nPa; however, we can notice that, if we compare the NH and SH reconfigurations at rotation A with those at rotation C, no important difference is seen, as regards both their morphologies and their timings. In conclusion, it seems reasonable to conclude that the dynamic pressure does not play a significant role in determining the convection reconfiguration times during this event. On the other hand, it cannot be excluded that such a role could be important in other events which display dynamic pressure changes in combination with IMF rotations.

In the NH the SuperDARN data coverage was extensive enough to base the description of the convection reconfiguration on the maps obtained through the map potential technique, while in the SH we made use of individual plots of the TIGER V_{LOS}. Moreover, in Sect. 6 we further investigated such response by considering V_{LOS}'s measured in the two hemispheres in two nominally conjugated regions between 11 and 12 MLT. We found that the two hemispheres display similarities and differences which need to be commented upon and discussed.

7.1 $B_y > 0$ **convection patterns**

We discuss first the observed topology of the patterns for the IMF $B_y > 0$ dominated configuration, i.e. after rotations A and C and prior to rotations B and D. In all such cases the NH pattern was dominated by a large clockwise cell extending from the dusk side to the dawn side (Cowley and Lockwood, 1992). For the SH we notice that the TIGER V_{LOS} was consistent with the presence of a duskward-tailward flow between 76° and 82° MLAT; at the same time the data provided by the night side SuperDARN radars complemented the morning side measurements by TIGER, so that the map potential software steadily reconstructed a large counterclockwise cell on the morning side, extending partly to the dusk side, characterised by a smaller clockwise cell (see panels 2 and 4 from the top of Fig. 6). The obvious interpretation of these patterns is that they are generated by $B_y > 0$ day side reconnection, that pulls reconnected field lines from dusk to dawn in the NH and from dawn to dusk in the SH. Nothing more can be said about further features of the SH pattern due to the paucity of the data. On the contrary, the NH patterns also showed evidence of secondary cells, similarly to what was already observed by other authors. In this regard, we re-

call that a smaller dawn side counter-clockwise cell was often observed in the NH, sometimes completely formed, other times only partially resolved due to the incomplete MLT and MLAT coverage. In two cases we also observed three cell structures, i.e. at 22:18–22:20 UT (Fig. 2) and at 22:46–22:48 UT (Fig. 3), which seem to match the model of Reiff and Burch (1985). To this regard, we also remark that the 22:18–22:20 UT three cell pattern developed from the four cell pattern of 22:06–22:08 UT through the 22:10–22:12 UT map. This sequence of convection maps resembles closely the past observations by Huang et al. (2000b), who observed that, as IMF B_y became more dominant, the reverse cells shifted in MLT, reducing the size of one of the cells until a three-cell convection pattern developed.

7.2 $B_z > 0$ **convection patterns**

Under $B_z > 0$ conditions, i.e. prior to rotation A, between rotations B and C and after rotation D, in general the NH patterns show signatures of two large reverse cells (see e.g. Milan et al., 2000; Huang et al., 2000a). Prior to the first rotation, such cells are both clearly reconstructed, while in the other cases the dusk counter-clockwise cell is not completely formed and the dawn cell can only be inferred from the general shape of convection. We explain such a pattern as due to high latitude lobe reconnection as expected for a mainly northward IMF. However, we recall that a low latitude dawnward flow, mainly across the noon MLT meridian, is always present, with variable intensity and, at times, with a tailward component. This flow coexists with lobe cells, even when two such cells are clearly observed at the same time, and can be interpreted as a distortion of the reverse convection pattern due to the prevailing positive B_y; on the other hand, it could also be that, as B_y is steadily positive, the lobe reconnection line extends to the day side, duskward of the cusp (see e.g. Sandholt et al., 2003). Finally, we remark that, prior to rotation A, for several minutes, as illustrated in Fig. 2 in the 22:06–22:08 UT panel, we observed clear signatures of a four cell system, composed of two central reverse cells (roughly symmetric relative to noon MLT) accompanied by two lower latitude viscous cells as suggested by Reiff and Burch (1985) and observed by Huang et al. (2000a).

As regards the SH, careful visual inspection of all TIGER FOV plots showed that the velocity patterns under $B_z > 0$ conditions are very different from those seen under dominant $B_y > 0$ conditions. This is evident from panels 1, 3 and 5 of Fig. 6, which are typical of the periods before rotation A and C and after rotation D. In all three periods TIGER observes both positive and negative V_{LOS}: in panels 3 and 5 the positive V_{LOS}'s form two spots at dawn roughly at the same MLT and MLAT; in panel 1 they form a spot closer to 12:00 MLT. The three spots can be interpreted as signatures of flow moving from high to low latitude, i.e. with a sunward component. Moreover, in panels 3 and 5 the positive V_{LOS} spot occurs between two negative V_{LOS} spots, at dawn and

dusk of it, respectively, which are compatible with the signature of two reverse lobe cells. Such a signature is not seen in panel 1, which only displays sparse echoes in the rest of the dawn quadrant and none at all in the dusk quadrant. Although the data coverage is low, it is clear that the TIGER observations under $B_z > 0$ conditions are very different from those pertaining to dominant $B_y > 0$ conditions. In conclusion, we suggest that both in the NH and in the SH reverse lobe cells are formed under $B_z > 0$ conditions, although for the SH the evidence is not so compelling as for the NH.

7.3 Relation between the number of radar echoes and IMF orientation

We shall now discuss the result shown in the bottom panel of Fig. 7, concerning the evolution of the number of echoes observed in the TIGER and Kodiak FOV's as a function of IMF orientation.

Other authors have discussed in the past the rate of occurrence of SuperDARN backscatter as a function of season, MLT, MLAT and geomagnetic activity. For our purposes it is useful to cite Ruohoniemi and Greenwald (1997), who described a marked seasonal effect in the rate of backscatter, found that such rates are much lower in summer than in winter, and "attributed this dependence to the suppression of density gradients by more intense photoionisation in summer". These remarks were confirmed, among others, by Milan et al. (1997), and by Vickrey and Kelley (1982) and Kelley et al. (1982), who noticed that increased conductivity in the E layer due to summer insolation can favour the decay of F-region density gradients. We rest on such considerations to explain why, in our case, TIGER observes a much smaller number of echoes than Kodiak throughout the event: the TIGER FOV is constantly illuminated by sunlight, so that day side ionisation smooths out the ionospheric density irregularities. Conversely, the Kodiak FOV is constantly beyond the day-night terminator, where density irregularities are much more probable and long lived.

Moving to the issue of the dependence of the rate of scatter on the IMF orientation, we recall that Ballatore et al. (2000) argued that reconnection at the magnetopause yields an increase of ionospheric irregularities, which are responsible for the generation of HF backscatter. It is by this same argument that we may try to address the different behaviour of N_T and N_K in response to the IMF rotations, as evidenced in Fig. 7. Starting from the Kodiak radar, we notice that the conditions were favourable to HF backscatter as in its FOV more than 150 echoes were observed throughout the event. In particular, about 200 echoes were observed already at the beginning of the event, under positive B_z conditions, when particle precipitation probably occurred along field lines due to both lobe reconnection and to low latitude reconnection associated to the large positive B_y component (as argued in the preceeding subsection). It is not inconceivable that, in such a situation, strong precipitations associated to reconnection might pro-

duce two competing effects in the ionosphere: on one side to increase the density irregularities in the F-region, on the other side to worsen the local propagation conditions. As a result, as we remarked already in Sect. 6, the total number of echoes observed by Kodiak in its FOV, N_K, does not change as much as for TIGER during the event; moreover, although a dependence of N_K on the IMF orientation is observed, this is less clear than for N_T.

The situation is different for the TIGER FOV. In this case the number of echoes is around 50 under positive B_z conditions and around 100–150 under B_y dominated conditions and displays time variations anti-correlated (with a -0.86 correlation coefficient at 2 min lag) with those of V_T displayed in the upper panel of Fig. 7. Actually, N_T is not equivalent to V_T, as N_T pertains to the whole TIGER FOV, while V_T pertains to a limited region, between 11:00 and 12:00 MLT and $-78°$ and $-80°$ MLAT. Therefore, for this event we take N_T as an additional indicator of the SH reconfiguration.

If we look back at panel 1 of Fig. 6, we see that most echoes concentrated in two small MLT-MLAT spots between 11:00 and 12:00 MLT, with positive and negative velocities. It is natural to interpret such echoes as due to local irregularities caused by particle precipitation along field lines from a lobe reconnection site close to the southern cusp, as this is the only place in the TIGER FOV where irregularities are likely to occur under the present conditions of solar illumination. The problem may be posed of whether lobe reconnection occurs at all at the southern magnetopause under the given conditions, as the dipole tilt should favour the SH hemisphere, but the negative IMF B_x component could favour the NH instead. We do not have any means of checking this directly, as no low altitude spacecraft was flying at the right place at this particular time, while the Cluster fleet was on an outbound orbit in the northern magnetosphere. However, we made use of the Cooling et al. (2001) model to check the probability that component merging may take place tailward of the southern cusp and found that a small SH lobe merging line could develop for all the positive B_z conditions present during our event. Actually, we ran the Cooling model for the NH too and found that lobe reconnection is more probable there.

Following this line of thought, we can proceed to interpret the increase of N_T which occurs between 22:12 and 22:18 UT. We suggest that the SH convection reconfigures after the A rotation and a dawn side low latitude merging line sets up, as expected for dominating $B_y > 0$. Under these conditions the increase of the number of echoes is just the effect of the increased reconnection at low latitude (Ballatore et al., 2000). The same should apply to the increase observed soon after the C rotation. On the opposite, the decrease of N_T observed after the B and D rotations can be interpreted in terms of the switching off of the low latitude reconnection with the simultaneous start of a weak lobe reconnection.

Table 2. Start and End times of NH and SH convection reconfigurations following the A, B, C and D IMF rotations. Derived delays between start times are also listed (see text for details).

rot. (UT)	NH Start(UT)	NH End(UT)	SH Start(UT)	SH End(UT)	ΔStart(min)
A 22:08	22:08	22:14	22:08	22:14	0
C 23:18	23:18	23:24	23:18	23:22	0
B 22:45	22:45	23:02	22:58	23:04	13
D 23:55	00:04	00:18	00:12	00:20	8

7.4 NH and SH reconfiguration times

Early models and observations suggested that IMF rotations cause the reconfiguration of ionospheric convection on time scales of tens of minutes starting from the noon sector (Lockwood et al., 1986; Todd et al., 1988; Saunders et al., 1992).

In Sects. 4 and 5 we suggested that, during the period that we have analysed, the time it takes for the convection maps to respond to an IMF rotation and to reconfigure depends both on the IMF and on the hemisphere and is larger for the SH when the IMF rotates from dominant $B_y > 0$ to $B_z > 0$. Before further discussing this suggestion, it is necessary to comment on the doubts that could be raised about it due the scarcity of SH data, as, in principle, we cannot totally exclude that reconfiguration started in the SH at an earlier time at a different MLAT-MLT location and then suddenly, i.e. within less than 1 min, moved to the place where TIGER actually detected it. To this regard, we recall that negative $V_{\rm LOS}$'s (i.e. duskward-tailward) were observed by TIGER over an extended MLAT-MLT region both before rotations B and D, and after such rotations, for several minutes, at times when the NH reconfiguration had already clearly started; moreover, the reconfiguration was observed in the TIGER data roughly at the centre of the existing region of tailward-duskward flow, roughly at the location where one would expect the formation of a new lobe merging line under the current IMF conditions, both according to the general picture of ionospheric convection and according to the calculations we made through the Cooling et al. (2001) model (see Sect. 7.3). Therefore, it is natural to interpret the observations in terms of a SH reconfiguration actually starting first where TIGER actually saw it.

To complement the considerations on reconfiguration times based on NH convection maps and on SH TIGER FOV plots of $V_{\rm LOS}$, in Sect. 6 we looked at $V_{\rm LOS}$'s reversals observed near noon MLT in the NH and in the SH by the Kodiak and the TIGER radar respectively and found that: 1) the IMF rotations towards B_y dominated are accompanied by simultaneous NH and SH fast reconfigurations within a few minutes after the nominal IMF rotation; 2) the response to IMF northward rotations is slower, by several minutes; 3) the response to IMF northward rotations occurs in the NH about 8–13 min earlier than in the SH. Such results must be regarded as additional evidence of the validity of the interhemispheric

reconfiguration times evaluated on the basis of convection maps and TIGER FOV plots. Unfortunately, the Sect. 6 analysis could not be extended quantitatively to other MLT's and MLAT's because of the presence of gaps, especially in the SH data. However, as we discussed in Sect. 7.3, a support to our interpretation of the reconfiguration times comes also from the time evolution of the N_T and N_K parameters, which display a behaviour anticorrelated to that of V_T and V_K.

Table 2 summarises our observations based on convection maps and TIGER FOV plots of $V_{\rm LOS}$. The two top lines refer to the A and C rotations, when the IMF turned from $B_z > B_y > 0$ to $B_y > |B_z|$, while the two bottom lines refer to the opposite IMF rotations, B and D. For each rotation Table 2 shows the start and end times of reconfiguration in the NH and in the SH, together with the delay between the NH and SH start times, ΔStart. As the time resolution is much higher for the IMF than for SuperDARN maps, we do not assign an error to the A, B and C times. As regards rotation D, we selected the start of the rotation which we know lasted for 20 min. As the times under the Start and End headings were determined from convection maps in Sects. 4 and 5, they should all be assigned a 2-min error. As a consequence, ΔStart's should be assigned a maximum 4-min error.

It appears that for the A and C rotations the start times of the reconfigurations were very similar for the NH and for the SH, within 2 min. Moreover, the reconfigurations seem to have started at the nominal IMF rotation time. To this regard, we recall that the timing of the A and C IMF turnings can be affected by large errors, as we noted in the presentation of Fig. 1. Finally, we remark that the reconfiguration times were rather fast, on the order of 6 min, suggesting that the low latitude B_y driven reconnection starts roughly at the same time in both hemispheres and influences very rapidly the whole day side ionosphere. This result seems to agree with the observations by Ruohoniemi and Greenwald (1998) and Shepherd et al. (1999), who showed cases when the reconfiguration from strong northward IMF convection to strong southward IMF convection occurred in 2–4 min simultaneously at all MLT's extending from noon to midnight.

Regarding the B and D IMF rotations, it appears that the time response is quite different for the NH and the SH. In fact, we observe that in the SH the reconfiguration starts considerably after the IMF nominal rotation (13 and 17 min for rotation B and D respectively) and lasts on the order of

6–8 min. Conversely, in the NH the reconfiguration starts earlier (0 and 9 min after the IMF nominal time for rotations B and D respectively), but lasts much longer, 14–17 min, so that the SH completes the reconfiguration only a few minutes after the NH. This result is compatible with earlier findings by Taylor et al. (1998), who used NH SuperDARN convection velocities to show that sunward flows appeared in the noon sector within 2 min following an IMF northward turning and that the global flow completely reconfigured in 20 min, and by Huang et al. (2000a), who found that the NH reverse convection cells form within $\simeq 12$ min after a northward turning of the IMF. In conclusion, the new result of our work is the late start and the faster reconfiguration observed in the SH at rotations B and D.

We summarise the sequence of events observed for both the B and the D rotations: 1) appearance in the NH of a clockwise cell centred at 10:00–10:30 MLT and 82° MLAT; 2) strengthening of the new NH cell; 3) appearance in the NH of a sunward flow channel from the polar cap (bending towards dawn at or below 80°); 4) sudden reconfiguration of the SH pattern with the appearance of a flow from high to low latitude between 11:00 and 12:00 MLT; 5) completion of the NH reconfiguration and, within minutes, appearance of SH signatures of two reverse cells.

To this regard, we recall that, as this event occurred in winter time, the magnetic dipole tilt should favour lobe reconnection in the SH; however, a large B_x is believed to alter this seasonal effect (Cowley, 1983; Crooker and Rich, 1993; Lockwood and Moen, 1999). This is exactly the case for the event that we have described in this work, as at rotation B ACE B_x changed from $\simeq -3$ nT to $\simeq -10$ nT and at rotation D it changed from $\simeq -3$ nT to $\simeq -7$ nT, while both at B and D ACE B_z changed from $\simeq -3$ nT to $\simeq 10$ nT and B_y changed from $\simeq 10$ nT to $\simeq 0$ nT. As a last remark, it is worth recalling that, following Østgaard et al. (2005), for a northward IMF, positive IMF B_x "may cause reconnection to occur first and more efficiently in the southern lobe". If we adopt this argument for our event, we must conclude that negative B_x at the B and D rotations can be invoked to explain the fact that the ionospheric reconfiguration occurs in the NH earlier than in the SH. To this regard, we may also recall that Provan et al. (2005) argued that "reconnection in the unfavoured hemisphere may eventually be activated at a later stage, involving the overdraped magnetic flux." We are at present unable to estimate the time delay which we should expect in our event between northern and southern lobe reconnection and leave this investigation to a future study. However, we can also think of other possible causes of the observed delay. Firstly, one could think of different positions of the lobe reconnection site in the NH and SH which could yield two different propagation times of the magnetosheath plasma to each site. Secondly, we could think of asymmetric propagation of the plasma in the two hemispheres, e.g. with a plasma stagnation in front of the southern cusp indentation, which would lead to a longer travel time to

the SH reconnection site. Thirdly, different conditions in the NH and SH ionospheres could yield different time responses to magnetopause reconnection. To this regard, throughout the event we have studied, the dayside ionospheric conductivity is certainly on average higher in the SH than in the NH ionosphere; however, it is not clear how such different conditions could be at work at rotations B and D of the IMF and not at rotations A and C. The investigation of these possibilities goes beyond the aim of this paper.

8 Summary and conclusions

We studied high-latitude convection during an interval of prolonged IMF $B_y > 0$ and found, as expected from previous works by other authors (Reiff and Burch, 1985), that the day side ionospheric convection is controlled by the IMF in both hemispheres.

For strongly northward IMF, we observed signatures of two reverse cells, both in the NH and in the SH, with sunward flow over the polar cap due to reconnection occurring tailward of the cusps. On one occasion we also observed in the NH two viscous cells at the sides of the central reverse cell pair, i.e. a four cell pattern.

For a dominating duskward IMF, we observed: in the NH a large dusk cell, accompanied by a smaller dawn cell and, on two occasions, a three cell pattern, composed of a large clockwise cell and two viscous cells (Reiff and Burch, 1985); in the SH a dawn cell protruding to the dusk quadrant, and, in one case, a smaller dusk clockwise cell. To a zero order approximation the NH and the SH patterns appeared to be symmetric.

The timings of the NH and SH convection reconfiguration after each IMF rotation were studied by comparing single NH convection maps before and after the A, B, C and D rotations with all TIGER FOV plots of V_{LOS}. This comparison showed that the convection reconfiguration from a $\theta \simeq 45°$ to a $\theta \simeq 90°$ pattern occurred almost simultaneously (i.e. within a few minutes) in the two hemispheres, as expected, because the magnetosheath draping over the day side magnetopause of a duskward IMF should give approximately simultaneous effects in the NH and SH.

On the contrary, we found that the reconfiguration from a B_y dominated to a northward IMF pattern starts in the NH 8–13 min earlier than in the SH. However, it appears that in the NH the reconfiguration occurs more slowly than in the SH (14–17 min compared to 6–8 min), so that eventually they are completed almost simultaneously.

We also studied the timing of convection reconfiguration between 11:00 and 12:00 MLT as seen by the NH Kodiak radar, between 78° and 80° MLAT, and as seen by the SH TIGER radar, between −78° and −80° MLAT, and found results compatible with the already mentioned global delay times. Moreover, we found that, for this period, the number of total echoes measured by TIGER in its FOV provides

an additional means of evaluation of the SH reconfiguration times.

In order to explain the observed delay in starting the reconfiguration in the two hemispheres, we suggest that: a) due to the presence of a strong negative IMF B_x component, a northward-tailward magnetosheath magnetic field starts reconnecting at the northern high latitude magnetopause, tailward of the cusp; b) the magnetic field is draped around the day side magnetopause; c) later on, the draped magnetic field reconnects at the high latitude southern magnetopause tailward of the cusp. Further to that, other contributions to the delay could be at play, e.g. asymmetric solar wind travel times in the NH and SH magnetosheath, asymmetric locations of the lobe reconnection sites, different conditions of the NH and SH ionosphere. The investigation of such possibilities lies beyond the aim of this paper.

The findings on different interhemispheric time responses to IMF rotations and on the SH variation of the backscatter rate with IMF orientation constitute the main and new results of this paper, which call for further studies based on similar events.

References

Amata, E., Ambrosino, D., Marcucci, M. F., and Coco, I.: Multi-instrument study of high latitude ionospheric convection during a positive By period, SIF, Conf. Proceedings, 11 Workshop Italian Research on Antarctic Atmosphere, edited by: Colacino, M. and Rafanelli, C., 79, 155–169, 2009.

Ballatore, P., Villain, J. P., Vilmer, N., and Pick, M.: The influence of the interplanetary medium on SuperDARN radar scattering occurrence, Ann. Geophys., 18, 1576–1583, 2000, http://www.ann-geophys.net/18/1576/2000/.

Balogh, A., Dunlop, M. W., Cowley, S. W. H., Southwood, D. J., Thomlinson, J. G., Glassmeier, K. H., Musmann, G., Luhr, H., Buchert, S., Acuna, M. H., Fairfeld, D. H., Slavin, J. A., Riedler, W., Schwingenschuh, K., and Kivelson, M. G.: The Cluster Magnetic Field Investigation, Space Sci. Rew., 79, 65–91, 1997.

Burke, W. J., Kelley, M. C., Sagalyn, R. C., Smiddy, M., and Lai, S. T.: Polar cap electric field structures with a northward interplanetary magnetic field, Geophys. Res. Lett. 6, 21–24, 1979.

Chisham, G., Lester, M., Milan, S. E., Freeman, M. P., Bristow, W. A., Grocott, A., McWilliams, K. A., Ruohoniemi, J. M., Yeoman, T. K., Dyson, P. L., Greenwald, R. A., Kikuchi, T., Pinnock, M., Rash, J. P. S., Sato, N., Sofko, G. J., Villain, J.-P., and Walker, A. D. M.: A decade of the Super Dual Auroral Radar Network (SuperDARN): scientfc achievements, new techniques and future directions, Surv. Geophys., 28, 33–109, 2007.

Cooling, B. M. A., Owen, C. J., and Schwartz, S. J.: Role of magnetosheath flow in determining the motion of open flux tubes, J. Geophys. Res., 106, 18763–18775, 2001.

Cowley, S. W. H.: Interpretation of observed relations between solar-wind characteristics and effects at ionospheric altitudes, in: High Latitude Space Plasma Physics, edited by: Hultqvist, B. and Hagfors, T., 225–249, Plenum, New York, 1983.

Cowley, S. W. H. and Lockwood, M.: Excitation and decay of solar wind-driven flows in the magnetosphere-ionosphere system, Ann. Geophys., 10, 103–115, 1992.

Crooker, N. U. and Rich, F. J.: Lobe cell convection as a summer phenomenon, J. Geophys. Res., 98, 13403–13407, 1993.

Freeman, M. P., Farrugia, C. J., Burlaga, L. F., Hairston, M. R., Greenspan, M. E., Ruohoniemi, J. M., and Lepping, R. P.: The Interaction of a Magnetic Could With the Earth: Ionospheric Convection in the Northern and Southern Hemispheres for a Wide Range of Quasi-Steady Interplanetary Magnetic Field Conditions, J. Geophys. Res., 98, 7633–7655, 1993.

Greenwald, R. A., Baker, K. B., Dudeney, J. R., Pinnock, M., Jones, T. B., Thomas, E. C., Villain, J.-P., Cerisier, J.-C., Senior, C., Hanuise, C., Hunsucker, R. D., Sofko, G., Koehler, J., Nielsen, E., Pellinen, R., Walker, A. D. M., Sato, N., and Yamagishi, H.: DARN/SUPERDARN: A Global View of the Dynamics of High-Latitude Convection, Space Sci. Rev., 71, 761–796, 1995.

Heppner, J. P. and Maynard, N. C.: Empirical high-latitude electric field models, J. Geophys. Res. 92, 4467–4489, 1987.

Huang, C.-S., Sofko, G. J., Koustov, A. V., Andre, D. A., Ruohoniemi, J. M., Greenwald, R. A., and Hairston, M. R.: Evolution of ionospheric multicell convection during northward interplanetary magnetic field with $|B_z/B_y| > 1$, J. Geophys. Res. 105, 27095–27107, 2000a.

Huang, C.-S., Murr, D., Sofko, G. J., Hughes, W. J., and Moretto, T.: Ionospheric convection response to changes of interplanetary magnetic field Bz component during strong B_y component, J. Geophys. Res., 105, 5231–5243, 2000b.

Kamide, Y., Richmond, A. D., Emery, B. A., Hutchins, C. F., Ahn, B. H., de la Beaujardire, O., Foster, J. C., Heelis, R. A., Kroehl, H. W., Rich, F. J., and Slavin, J. A.: Groundbased studies of ionospheric convection associated with substorm expansion, J. Geophys. Res., 99, 19451–19466, 1994.

Kelley, M. C., Vickrey, J. F., Carlson, C. W., and Torbert, R.: On the origin and spatial extent of high-latitude F region irregularities, J. Geophys. Res., 87, 4469–4475, 1982.

Lockwood, M., van Eyken, A. P., Bromage, B. J. I., Willis, D. M., and Cowley, S. W. H.: Eastward propagation of a plasma convection enhancement following a southward turning of the interplanetary magnetic field, Geophys. Res. Lett., 13, 72–76, 1986.

Lockwood, M. and Moen, J.: Reconfiguration and closure of lobe flux by reconnection during northward IMF: possible evidence for signatures in cusp/cleft auroral emissions, Ann. Geophys., 17, 996–1011, 1999, http://www.ann-geophys.net/17/996/1999/.

Lu, G., Richmond, A. D., Emery, B. A., Reiff, P. H., de la Beaujardière, O., Rich, F. J., Denig, W. F., Kroehl, H. W, Lyons, L. R., Ruohoniemi, J. M., Friis-Christensen, E., Opgenoorth, H., Persson, M. A. L., Lepping, R. P., Rodger, A. S., Hughes, T., McEwin, A., Dennis, S., Morris, R., Burns, G., and Tomlinson, L.: Interhemispheric asymmetry of the high-latitude ionospheric

convection pattern, J. Geophys. Res., 99, 6491–6510, 1994.

Milan, S. E., Yeoman, T. K., Lester, M., Thomas, E. C., and Jones, T. B.: Initial backscatter occurrence statistics from the CUT-LASS HF radars, Ann. Geophys., 15, 703–718, 1997, http://www.ann-geophys.net/15/703/1997/.

Milan, S. E., Lester, M., Cowley, S. W. H., and Brittnacher, M.: Dayside convection and auroral morphology during an interval of northward interplanetary magnetic field, Ann. Geophys., 18, 436–444, 2000, http://www.ann-geophys.net/18/436/2000/.

Newell, P. T. and Meng, C.-I.: Ionospheric projection of magneto-spheric regions under low and high solar wind pressure conditions, J. Geophys. Res., 99, 273–286, 1994.

Papitashvili, V. O., Belov, B. A., Faermark, D. S., Feldstein, Y. I., Golyshev, S. A., Gromova, L. I., and Levitin, A. E.: Electric-potential patterns in the northern and southern polar-regions paramaterized by the interplanetary magnetic field, J. Geophys. Res., 99, 13251–13262, 1994.

Provan, G., Lester, M., Grocott, A., and Cowley, S. W. H.: Pulsed flows observed during an interval of prolonged northward IMF, Ann. Geophys., 23, 1207–1225, 2005, http://www.ann-geophys.net/23/1207/2005/.

Reiff, P. H. and Burch, J. L.: IMF B_y-dependent flow and Birkeland currents in the day side magnetosphere. 2. A global model for northward and southward IMF, J. Geophys. Res., 90, 1595–1609, 1985.

Rich, F. J. and Hairston M.: Large-scale convection patterns observed by DMSP, J. Geophys. Res., 99, 3827–3844, 1994.

Ruohoniemi, J. M. and Greenwald, R. A.: Statistical patterns of high-latitude convection obtained from Goose Bay HF radar observations, J. Geophys. Res., 101, 21743–21763, 1996.

Ruohoniemi, J. M. and Greenwald, R. A.: Rates of scattering occurrence in routine HF radar observations during solar cycle maximum, Radio Sci., 32, 1051–1070, 1997.

Ruohoniemi, J. M. and Baker, K. B.: Large-scale imaging of high-latitude convection with Super Dual Auroral Radar Network HF radar observations, J. Geophys. Res., 103, 20797–20811, 1998.

Ruohoniemi, J. M. and Greenwald, R. A.: The response of high-latitude convection to a sudden southward IMF turning, Geophys. Res. Lett., 25, 2913–2916, 1998.

Ruohoniemi, J. M. and Greenwald, R. A.: Dependencies of high-latitude plasma convection: Consideration of inter-planetary magnetic field, seasonal, and universal time factors in statistical patterns, J. Geophys. Res., 110, A09204, doi:10.1029/2004JA010815, 2005.

Sandholt, P. E., Moen, J., Farrugia, C. J., Cowley, S. W. H., Lester, M., Milan, S. E., Valladares, C., Denig, W. F., and Eriksson, S.: Multi-site observations of the association between aurora and plasma convection in the cusp/polar cap during a southeastward ($B_y \sim |B_z|$) IMF orientation, Ann. Geophys., 21, 539–558, 2003, http://www.ann-geophys.net/21/539/2003/.

Saunders, M. A., Freeman, M. P., Southwood, D. J., Cowley, S. W. H., Lockwood, M., Samson, J. C., Farrugia, C. J., and Hughes, T. J.: Dayside ionospheric convection changes in response to long period IMF oscillations: Determination of the ionospheric phase velocity, J. Geophys. Res., 97, 19373–19380, 1992.

Shepherd, S. G., Greenwald, R. A., and Ruohoniemi, J. M.: A possible explanation for rapid, large-scale ionospheric responses to southward turnings of the IMF, Geophys. Res. Lett., 26, 3197–3200, 1999.

Shepherd, S. G. and Ruohoniemi, J.: Electrostatic potential patterns in the high-latitude ionosphere constrained by SuperDARN measurements, J. Geophys. Res., 105, 23005–23014, 2000.

Taylor, J. R., Cowley, S. W. H., Yeoman, T. K., Lester, M., Jones, T. B., Greenwald, R. A., Sofko, G., Villain, J.-P., Lepping, R. P., and Hairston, M. R.: SuperDARN studies of the ionospheric convection response to a northward turning of the interplanetary magnetic field, Ann. Geophys., 16, 549–565, 1998, http://www.ann-geophys.net/16/549/1998/.

Todd, H., Cowley, S. W. H., Lockwood, M., Willis, D. M., and Luhr, H.: Response time of the high latitude day side ionosphere to sudden changes in the north-south component of the IMF, Planet. Space Sci., 36, 1415–1428, 1988.

Vickrey, J. F. and Kelley, M. C.: The effects of a conducting E layer on classical F region cross-field plasma diffusion, J. Geophys. Res., 87, 4461–4468, 1982.

Weimer, D. R.: Models of high-latitude electric potentials derived with a least error fit of spherical harmonic coefficients, J. Geophys. Res., 100, 19595–19608, 1995.

Østgaard, N., Mende, S. B., Frey, H. U., Frank, L. A., and Sigwarth, J. B.: Observations of non-conjugate theta aurora, Geophys. Res. Lett., 32, L2125, doi:10.1029/2003/GL017914, 2003.